Synthesis and Characterization of Temperature and pH Responsive PIA-b-PNIPAM@Fe_3O_4 Nanocomposites

Swati Kumari , Olufemi Ogunjimi , Fatema Tarannum , Keisha B. Walters *

Posted Date: 20 May 2025

doi: 10.20944/preprints202505.1553.v1

Keywords: stimuli responsive; poly(itaconic acid); poly(N-isopropyl acrylamide); nanocomposite; temperature; pH

 doi:10.20944/preprints202505.1553.v1

Article

Synthesis and Characterization of Temperature and *pH* Responsive PIA-b-PNIPAM@Fe_3O_4 Nanocomposites

Swati Kumari [1], Olufemi Ogunjimi [2], Fatema Tarannum [2] and Keisha B. Walters [2,*]

[1] Operations Food Safety, Amazon, Santa Clara, CA 95054, USA

[2] Ral*pH* E. Martin Department of Chemical Engineering, University of Arkansas, Fayetteville, AR 72701, USA

* Correspondence: keisha.walters@uark.edu

Abstract: Stimuli-responsive polymers (SRPs) have garnered significant attention in recent decades due to their immense potential in biomedical and environmental applications. When these SRPs are grafted onto magnetic nanoparticles, they form multifunctional nanocomposites capable of various complex applications, including targeted drug delivery, advanced separations, and magnetic resonance imaging. In this study, we employed a one-step hydrothermal method using 3-aminopropyltrimethoxysilane (APTES) to synthesize APTES-modified Fe_3O_4 nanoparticles (APTES@Fe_3O_4) featuring reactive terminal amine groups. Subsequently, via two consecutive surface-initiated atom transfer radical polymerizations (SI-ATRP), *pH*- and temperature-responsive polymer blocks were grown from the Fe_3O_4 surface, resulting in the formation of poly(itaconic acid)-block-poly(N-isopropyl acrylamide) (PIA-b-PNIPAM) grafted nanomagnetic particles (PIA-b-PNIPAM @Fe_3O_4). To confirm the chemical composition and assess how particle morphology and size distribution of these SRP-based nanocomposites change in response to ambient *pH* and temperature stimuli, various characterization techniques were employed, including transmission electron microscopy (TEM), differential light scattering (DLS), and Fourier transform infrared spectroscopy (FTIR). The results indicated successful synthesis, with PIA-b-PNIPAM @Fe_3O_4 demonstrating sensitivity to both temperature and *pH*.

Keywords: stimuli responsive; poly(itaconic acid); poly(N-isopropyl acrylamide); nanocomposite; temperature; *pH*

1. Introduction

Polymers have been widely employed due to their exceptional properties, including high strength, durability, flexibility, and ease of processing, which make them suitable for various applications, including consumer products, coatings, electronics, sensors, actuators, optoelectronic devices, information storage, medical and engineering composites[1–8] .To function as smart materials, however, these polymers must demonstrate reversibility, visibility, and measurable responses to external stimuli such as mechanical stress, heat, light, gases, electricity, and *pH* changes. Stimuli-responsive polymers (SRPs), often referred to as "smart" polymers, possess structural features, such as responsive functional groups or moieties, that enable them to undergo reversible changes in their physical or chemical properties in response to such stimuli in a controllable manner[9]. For instance, thermoresponsive polymers like Poly(N,N-diethylacrylamide) (PDEAAm) exhibit a transition from hydrophilic to hydrophobic behavior with temperature changes[10], while pH-sensitive polymers like poly(acrylic acid) (PAA) alter their solubility in response to acidity variations[11,12]. This responsiveness has significantly expanded their application potential in fields like medicine, biosensing, drug delivery and diagnostics, image targeting, tunable catalysis, self-healing materials, and colloids, owing to their ability to provide controlled release, enhanced

 doi:10.20944/preprints202505.1553.v1

bioavailability, improved therapeutic specificity, reduced toxicity, and integrated theranostic capabilities[10,13–18].

A wide variety of water-soluble, non-fouling and biodegradable polymers such as poly(ethylene glycol) (PEG)[19,20], poly(ethylene oxide) (PEO)[21], dextran[22,23], poly(acrylic acid) (PAA)[24,25], poly (aspartic acid)[26], poly (methacrylic acid)[27,28], 3-methyl glutarylated poly[29], and poly (L-histidine)[30] have been explored for the fabrication of SRPs due to their tunable physicochemical properties and excellent biocompatibility. Among these, poly(N-isopropylacrylamide) (PNIPAM) is one of the SPRs, well-known for its dual sensitivity to *pH* and temperature[31–33], characterized by hydrophilic amide (-CONH-) groups and hydrophobic isopropyl (-CH(CH_3)$_2$) side chains. With a lower critical solution temperature (LCST) of ~32°C[34]—just below human body temperature (~37°C), PNIPAM undergoes a hydrophilic-to-hydrophobic transition. Below its LCST, the polymer remains swollen and hydrated, capable of entrapping hydrophilic drugs via hydrogen bonding[35]. When heated above the LCST, PNIPAM chains collapse due to dominant hydrophobic interactions, effectively releasing their cargo[36]. This behavior can also be modulated by copolymerizing PNIPAM with other monomers to shift its LCST above 37 °C [37]. On the other hand, research on poly(itaconic acid) (PIA) has been relatively limited, primarily because of its poor solubility in most organic solvents except methanol. Despite the limitation, its hydrophilicity, biocompatibility and pH-sensitive behavior[38,39]—attributed to the presence of ionizable carboxylic acid groups— make it a promising candidate for sustainable systems. In this study, the combination of PIA with thermoresponsive PNIPAM enables the development of dual-stimuli-responsive nanocomposites, suitable for targeted drug delivery, diagnostics, and environmental applications.

The synthesis of SRPs, particularly PNIPAM, has been achieved through various polymerization techniques, including free radical polymerization (FRP), redox polymerization, ionic polymerization, radiation polymerization, and living radical polymerization[40]. While FRP offers simplicity and scalability, it lacks control over critical macromolecular parameters such as molecular weight distribution, chain-end functionality, and architectural precision, which are essential for finely tuning the responsive behavior of PNIPAM[41]. Atom transfer radical polymerization (ATRP) has emerged as a superior alternative, enabling the synthesis of well-defined PNIPAM with narrow dispersity, tailored molecular weight, and complex architectures including block and graft copolymers[42]. An extension of ATRP, known as surface-initiated ATRP (SI-ATRP), facilitates spatially controlled polymer growth, high grafting densities, and uniform brush morphologies, making it particularly well-suited for fabricating surface-confined stimuli-responsive systems[43]. Yar et al.[44] utilized SI-ATRP to prepare PNIPAM-coated SPIONPs that exhibited dual *pH* and temperature responsiveness. These nanoparticles achieved ~90% release of doxorubicin (DOX) at *pH* 5 and 42 °C while remaining stable under physiological conditions, demonstrating their potential for MRI-guided cancer therapy. In this present study, a two-step SI-ATRP strategy was applied to synthesize block copolymers on superparamagnetic iron oxide nanoparticles (SPIONPs), aiming to improve the performance of PNIPAM-based SRPs.

SRPs have been increasingly combined with nanomaterials such as carbon nanotubes (CNTs)[45–47], graphene[48], and SPIONPs[49,50]—typically within the size range of ~20–250 nm —to engineer multifunctional platforms for applications including targeted drug delivery, medical diagnostics, bioimaging, and environmental monitoring. Table 1 provides a comprehensive overview of some recent studies on stimuli-responsive polymer composites, highlighting their synthesis strategies, functionalization techniques, and their tunable application because of their external stimuli such as pH, temperature, and magnetic fields. A near-infrared (NIR)-responsive nanocarrier was designed by encapsulating chitosan(CS)-coated single-walled CNTs within a PNIPAM hydrogel crosslinked with poly(ethylene glycol) diacrylate (PEGDA), denoted as CS/PNIPAM@CNT. This hybrid system exhibited high DOX loading efficiency (~43%) and demonstrated multi-stimuli-responsive drug release under elevated temperature (40 °C), acidic *pH* (5.0), and NIR irradiation, significantly enhancing cellular uptake and cytotoxic efficacy for targeted cancer therapy[51]. SPIONPs, in particular, offer significant advantages due to their high surface-to-volume ratio and

 doi:10.20944/preprints202505.1553.v1

superparamagnetic behavior, enabling their use in magnetic resonance imaging (MRI), magnetic hyperthermia, cell sorting, magnetically responsive drug delivery, controlled drug release and sensing applications [52–60]. For instance, Ramanujan and co-workers developed a PNIPAM hydrogel crosslinked with N,N′-methylenebis(acrylamide) (MBAm), and embedded with SPIONPs for alternating magnetic field (AMF)-triggered doxorubicin release, where localized heating induced hydrogel contraction to enable controlled drug delivery[61]. In another study, Toma et al. developed a surface plasmon resonance (SPR) biosensor with a 3D biomolecular interface, based on a PNIPAM-based thermoresponsive hydrogel integrated with an indium tin oxide (ITO) microheater, enabling rapid and reversible SPR signal modulation through temperature-induced changes in volume and refractive index[35]. Additionally, Karthika et al. developed a chitosan polymer based nanocomposite incorporating SPIONPs with reduced graphene oxide, resulting in high drug-loading capacity and magnetically controlled drug release[62]. However, NPs' intrinsic tendency to agglomerate, driven by strong dipole–dipole interactions, poses challenges for colloidal stability. Therefore, surface modification is crucial to enhance their dispersibility, biocompatibility, and ensure uniform distribution within polymeric composite networks. Aminopropyltrimethoxysilane (APTES), a widely used silane coupling agent, contains three hydrolyzable ethoxy groups that undergo silanization, forming stable Si–O bonds with the Fe_3O_4 nanoparticle surface, and the terminal amine group ($–NH_2$) acts as reactive site for grafting polymers[53] such as PIA and PNIPAM. This functionalization enhances the integration and dispersion of iron oxide nanoparticles into polymer network, thereby improving the performance of nanocomposites in biomedical and sensing applications.

In this study, initially, Fe_3O_4 nanoparticles were synthesized in-house using a one-step hydrothermal technique, followed by surface modification with 3-aminopropyltrimethoxysilane (APTES) to introduce reactive amine groups onto the nanoparticle surface. Unlike previous studies that utilized commercially available nanoparticles, the in-house synthesis helped to minimize the breakage and aggregation of NPs. Then, two successive surface-initiated atom transfer radical polymerization (SI-ATRP) steps were performed to prepare a dual-responsive (*pH* and temperature) block copolymer, poly (itaconic acid)-b-poly(N-isopropylacrylamide) (PIA-b-PNIPAM) onto the surface of APTES-modified Fe_3O_4or amine functionalized Fe_3O_4 NPs. APTES modification allows the polymer chains to grow extend outward from the nanoparticle surface minimizing the entanglement and improve colloidal stability. The chemical composition, structure, *pH* and temperature responsiveness, and morphology of the PIA–b-PNIPAM@Fe_3O_4 nanoparticles were characterized using Fourier transform infrared spectroscopy (FTIR), dynamic light scattering (DLS), and transmission electron microscopy (TEM). Building upon our previous work involving PNIPAM-b-PIA grafted onto APTES@Fe_3O_4 via SI-ATRP[63] for thermoresponsive applications, this study further investigates the dual stimuli-responsiveness (*pH* and temperature dependence) of these nanocomposites for potential biomedical applications. The synthesized SRP-based nanocomposites show strong potential for use in advanced drug delivery systems, including targeted drug delivery and magnetic hyperthermia ferrofluids (MHFs) for cancer therapy.

Table 1. Recent literature review on stimuli-responsive polymer composites with their intended applications.

Synthesis Method	Polymer used	Functionalization	MNP	Nanocomposite	Application	Reference
Graft polymerization	Chitosan and PEG	PNIPAM	-	Chitosan films	Intended for medium suppuration wounds	Conzatti et al. [64]
One-step precipitation	PNIPAM	DNAzyme	-	PNIPAM/DNAzyme	Promising application in	Li et al.

 doi:10.20944/preprints202505.1553.v1

polymerization					biocatalysts (bioassays and biosensors)	
Polymerization of soap-free emulsion	NIPAM and acrylic acid (AA)	Thiol- and carboxyl-functionalized	Bimetallic (Cu/Pd)	PNIPAM-based bimetallic Cu/Pd	Possible application as hybrid catalytic materials in the synthesis of nitrogenous compounds with improved optical properties	Kakar et al. [65]
Thermal polymerization	Itaconic acid (IA)	Laponite RD	-	Nanocomposites hydrogels	Removal of cationic dyes	Huerta-Angeles et al.[66]
Radical polymerization	PNIPAM	PIA	Fe_3O_4-NPs	NIPAM-co-IA@Fe_3O_4	Possible application as a nanocarrier for targeted doxorubicin delivery.	Ghorbani et al. [67]
Hydrothermal approach	N-Isopropylacrylamide	-	Nickel ion doped iron oxide NPs	$NiFe_2O_4$-PNIPAM or FM	Application as a template for the efficient recovery of cefixime and methylene blue	Anushree et al. [68]
Radical polymerization	PNIPAM	APTES and β-Alanine	MNP	Poly(NIPAM-co-AA)	The research study compared the 'grafting to' and the 'in situ' method	Sakai et al. [69]
Co-polymerization	PNIPAM	Poly(itaconic acid) (PAA)	TiO_2@SiO_2	PNIPAM/PIA-TiO_2@SiO_2	Investigation for antibacterial activities against gram-	Mohamed and Hassabo[70]

 doi:10.20944/preprints202505.1553.v1

					positive and gram-negative bacteria (S. aureus and E. coli)	
Surface-initiated ATRP	PNIPAM	-	Fe_3O_4-NPs	SPION-PNIPAM	Application in contrast generation in MRI	Yar et al. [44]
Surface-initiated atom transfer radical polymerization	PNIPAM	Poly (itaconic acid) (PAA)	Fe_3O_4-Ps	Fe_3O_4-PIA-b-PNIPAM	Demonstration of the stimuli-responsive features (thermos-responsiveness) of the nanocomposites	Eyiler and Walters

2. Experimental

2.1. Materials

Iron (III) chloride hexahydrate ($FeCl_3.6H_2O$, CAS # 10025-77-1, 97%), sodium hydroxide (NaOH, ≥98%, anhydrous pellets), N-isopropyl acrylamide (NIPAM, ≥99%), itaconic acid (IA, ≥99%), 2,2'-bipyridyl (bpy, ≥99%), anhydrous 2-propanol (≥99.5%), and 3-aminopropyltrimethoxysilane (APTES, CAS #13822-56-5, 97%) were procured from Sigma-Aldrich. Ammonium hydroxide (NH_4OH), ethanol, trimethylamine (TMA, CAS #75-50-3, ≥99%), and 2-bromopropionyl bromide (BPB, CAS # 563-76-8) were purchased from Thermo Fisher Scientific. All chemicals were used as received without further purification unless otherwise specified. Millipore (Type I) water with a resistivity of 18.2 MΩ·cm was used in all experiments.

2.2. Synthesis of APTES Modified Fe_3O_4 Nanoparticles

Superparamagnetic iron oxide nanoparticles (SPIONPs) were synthesized via a one-step 3-aminopropyltrimethoxysilane (APTES) hydrothermal approach in order to achieve APTES-modified Fe_3O_4 nanoparticles bearing reactive terminal amine groups[53] as shown in Figure 1. A solution was prepared by dissolving 1.25 g of $FeCl_3{\cdot}6H_2O$ in 7.75 mL of deionized (DI) water, followed by stirring at 300 rpm for 10 min. Simultaneously, 6.25 mL of ammonium hydroxide (NH_4OH) was added dropwise under continuous stirring. The resulting mixture was then combined with 2.5 mL of APTES and transferred into a hydrothermal reactor, which was subsequently sealed. The reactor was placed in a preheated oven at 134 °C and maintained at this temperature for 3 h. After the reaction, the obtained product was washed three times with DI water and twice with ethanol using a 2T magnet for separation. The purified nanoparticles, denoted as APTES modified Fe_3O_4 or APTES@Fe_3O_4, were then sonicated and dispersed in water at a final concentration of 1 mg/mL.

 doi:10.20944/preprints202505.1553.v1

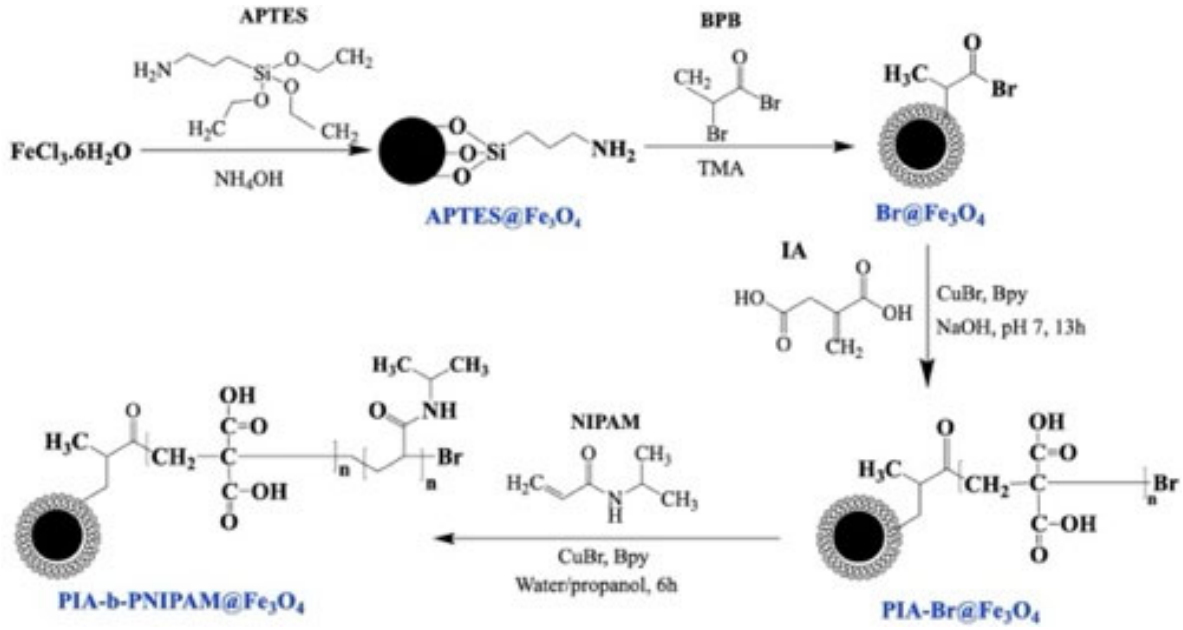

Figure 1. Schematic illustration of reaction mechanism of APTES modified Fe_3O_4 (APTES@Fe_3O_4) and PIA-b-PNIPAM@Fe_3O_4 via hydrothermal approach and surface initiated ATRP (SI-ATRP). APTES: 3-aminopropyltrimethoxysilane, BPB: 2-bromopropionyl bromide, IA: itaconic acid, NIPAM: N-isopropyl acrylamide.

2.3. Surface-Initiated Block Copolymerization of Itaconic acid (IA) and N-Isopropyl Acrylamide (NIPAM) on Fe_3O_4 Nanoparticles

An aliquot of 0.25 mL APTES modified Fe_3O_4 (APTES@Fe_3O_4) or amine functionalized Fe_3O_4 nanoparticles in aqueous solution, was vacuum-dried in a Schlenk flask. Subsequently, 1 ml of trimethylamine (TMA) (83.6 µL, 0.5 mmol) was added at approximately 0 °C, followed by the dropwise addition of 5 ml of 2-bromopropionyl bromide (52.4 µL, 0.5 mmol). The reaction mixture was stirred overnight at room temperature. The bromine-initiated NPs (Br@ Fe_3O_4) were then isolated using a 1.32T magnet, washed with ethanol, sonicated three times and subsequently dried under vacuum at room temperature.

Separately, a 1 M solution of itaconic acid (IA) (2.602 g, 20 mmol) was prepared in 15 mL of HPLC-grade water and deprotonated using NaOH (1.64 g) to adjust the *pH* to 7. Immediately after, 2,2'-bipyridyl (bpy) (62.5 mg, 0.4 mmol) and anhydrous 2-propanol (5 mL) were added, followed by sonication for 10 minutes. Dissolved oxygen was extracted using three freeze-pump-thaw cycles. Following the addition of Cu(I)Br (28.7 mg, 0.2 mmol) to the frozen solution, two additional cycles were performed. The solution was then left to polymerize for 13 h. The resulting PIA-grafted NPs (PIA-Br@Fe_3O_4) were purified by washing three times with water (H_2O) and left to settle under magnetic separation. The NPs were subsequently dried under vacuum.

Next, NIPAM (2.263 g and 20 mmol) was dissolved in a mixture of anhydrous 2-propanol/HPLC water (at 3:1 v/v, total volume at 20 ml). 2,2-bipyridyl (bpy) (62.5 mg, 0.4 mmol) and Cu(I)Br (28.7 mg and 0.2 mmol) were then quickly added to the mixture after three freeze-pump-thaw cycles. Two additional freeze-pump-thaw cycles were done to degas the mixture before 10 min sonication. The reaction mixture was polymerized for 6 h and then exposed to air. The resulting PIA-b-PNIPAM-grafted NPs were separated using a magnet, and any remaining catalyst, unreacted monomer, and ungrafted polymers were removed through three successive washes with water and ethanol. Finally, the purified nanoparticles were dried under vacuum.

2.4. Characterization

 doi:10.20944/preprints202505.1553.v1

The APTES-modified Fe_3O_4 and PIA-b-PNIPAM@Fe_3O_4 samples were characterized by attenuated total reflectance Fourier transform infrared (ATR-FTIR) spectroscopy using a Thermo Electron 6700 instrument equipped with a mercury-cadmium-telluride (MCT-A*) detector and a KBr beam splitter, controlled by Omnic software (v8.1.10, Thermo Fisher Scientific Inc.). Spectra were collected over 800-4000 cm^{-1} at a resolution of 4 cm^{-1}, averaging 256 scans using a MIRacle-ATR accessory (Pike Technologies) with a ZnSe/diamond crystal. The samples were deposited as solution droplets and allowed to dry on the crystal surface to form a thin film of nanoparticles.

A Zeta PALS analyzer (Brookhaven Instruments Corporation, BIC) with a 659 nm laser was used to measure nanoparticle hydrodynamic size and distributions in water by dynamic light scattering at a 90° detection angle. Before the measurements, samples were sonicated for 5 min and then allowed to stabilize in the cuvette for 3 min. Five consecutive 5 min runs were performed to determine particle size based on the effective diameter. Data collection and analysis were performed using BIC Particle Solutions software (v2.0).

Transmission electron microscopy (TEM) studies were carried out using a JEOL 100CXII operated at 100 kV, with high-resolution images obtained with a JEOL 2100 at 200 kV. For sample preparation, the nanoparticles were sonicated in an ultrasonic bath for 5 min, then a droplet was deposited onto a carbon Formvar copper grid (Electron Microscopy Science), and air-dried in a ventilated hood.

3. Results and Discussion

The successful functionalization of APTES-modified Fe_3O_4 (APTES@Fe_3O_4) and PIA-b-PNIPAM@Fe_3O_4 samples was confirmed through FTIR spectroscopy, as shown in Figure 2. Distinct Si–O stretching bands at 1084 cm^{-1} and 1005 cm^{-1} indicate APTES attachment in APTES-modified Fe_3O_4 sample. A band at 1129 cm^{-1}, assigned to C–N stretching, further supports the silane coating. The presence of amino silane on the Fe_3O_4-NH_2 nanoparticle surface is evidenced by N–H stretching at 3389 cm^{-1} and Si–O–Si vibrations at 995 cm^{-1}. Finally, PNIPAM grafting in the PIA-b-PNIPAM@Fe_3O_4 sample is confirmed by characteristic peaks at 1635 cm^{-1} and 1513 cm^{-1} [71], corresponding to the C=O stretching of secondary amides and N–H stretching vibrations of amide groups, respectively, reinforcing the successful polymer modification.

 doi:10.20944/preprints202505.1553.v1

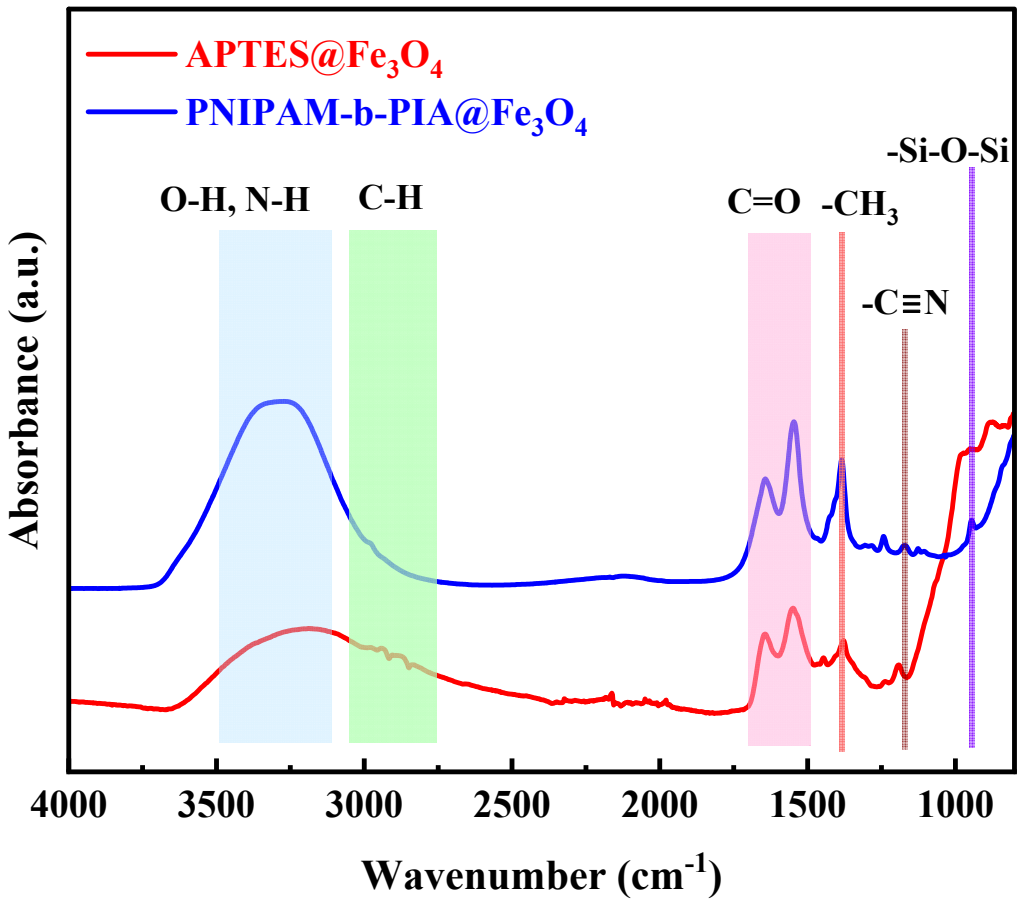

Figure 2. FTIR spectra of APTES@Fe_3O_4@ (red spectrum) and PIA-b-PNIPAM@Fe_3O_4 (blue spectrum).

Transmission electron microscopy (TEM) was performed to investigate the morphological characteristics of both APTES-modified Fe_3O_4 nanoparticles and surface-functionalized SRPs following two successive Surface-initiated atom transfer radical polymerization (SI-ATRP) reactions. Firstly, the polymerization of IA onto APTES-modified Fe_3O_4 (APTES@Fe_3O_4), was observed, as illustrated in Figures 3(a) and (b). The TEM images reveal the presence of a diffuse, hazy layer surrounding the iron oxide cores, indicative of the polymeric shell formed by PIA.

Subsequently, the synthesis of the block copolymer PIA-b-PNIPAM@Fe_3O_4 was confirmed by the polymerization of NIPAM, as shown in Figure 3(c) and (d) at different magnifications. The TEM micrographs distinctly depict the core-shell morphology, where the dark dense spherical core corresponds to Fe_3O_4 nanoparticles, and the surrounding lighter region to the PIA-b-PNIPAM structure. The observed particle size of ~ 1100 nm or ~ 1.1 μm confirms the significant increase in nanoparticle dimensions due to the successive polymerization steps, consistent with the hydrodynamic size measured by dynamic light scattering (DLS). The contrast variation between the core and shell regions in the TEM images further supports the successful encapsulation of the magnetic nanoparticles within the amphiphilic polymer matrix, reinforcing the efficiency of the SI-ATRP process in fabricating well-defined nanocomposites.

 doi:10.20944/preprints202505.1553.v1

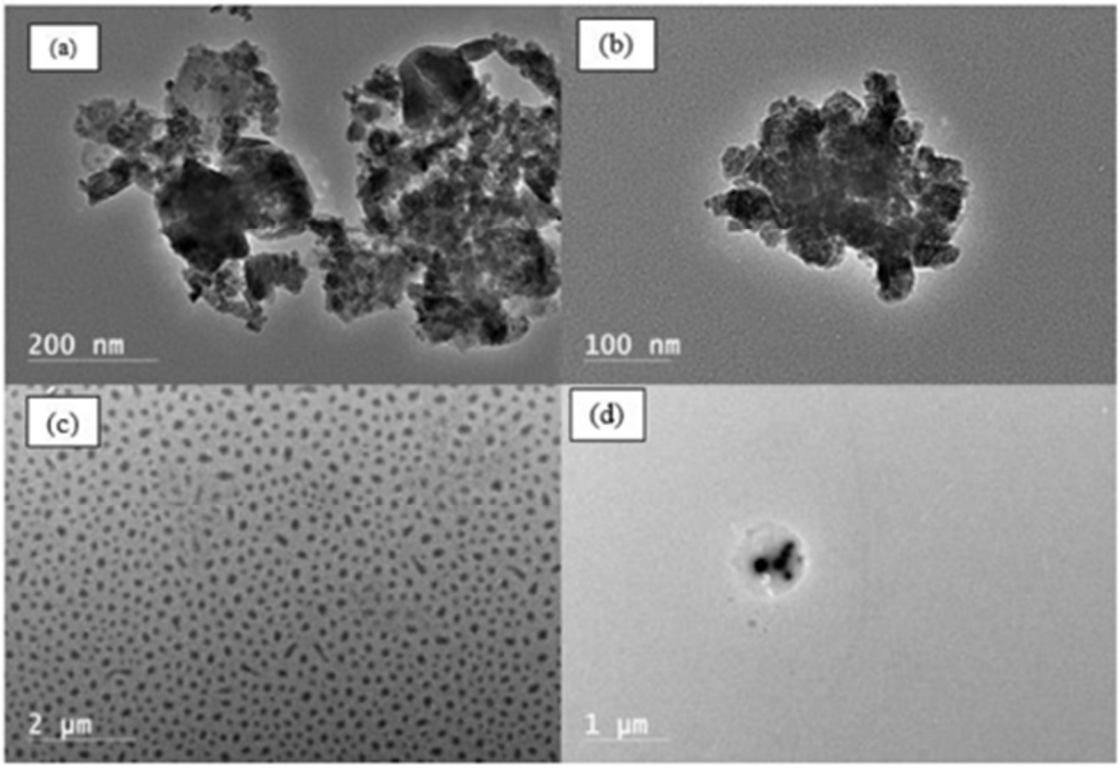

Figure 3. Transmission electron micrographs of APTES@Fe_3O_4 (a), PIA@Fe_3O_4 (b), and PIA-b-PNIPAM@Fe_3O_4 (c and d).

DLS data indicate that APTES@Fe_3O_4 nanoparticles had an average hydrodynamic diameter of 208 ± 2 nm. After grafting with PIA, the particle diameter increased significantly to 881 ± 8 nm, indicating successful formation of a PIA polymer shell around the magnetic core. Further modification to PIA-b-PNIPAM@Fe_3O_4 resulted in an additional size increase to 1164 ± 63 nm. This substantial growth suggests significant incorporation of PNIPAM as the secondary polymer block. In addition, both PIA and PNIPAM polymers are expected to be hydrated due to their hydrophilic nature and ability to swell in an aqueous environment. The observation in nanocomposite size aligns with expectations based on the polymer grafting process. Initially, the APTES coating on Fe_3O_4 provides a thin functional layer, minimally affecting the nanoparticle size. However, the introduction of a polyanionic polymer, PIA leads to a pronounced increase due to electrostatic repulsion and hydration effects, which contribute to the overall expansion of the polymer corona. The subsequent grafting of PNIPAM, further enlarges the nanoparticles, potentially due to additional hydration and chain extension in water at ambient temperatures.

Moreover, the DLS-measured hydrodynamic diameters correlate well with the TEM observations (as illustrated in Figure 3), where the core-shell structures of the nanoparticles are visually distinguishable. The difference between DLS and TEM measurements can be attributed to the hydration layer and polymeric swelling, as DLS assesses the hydrodynamic size in solution, while TEM provides a dry-state size measurement. This agreement between DLS and TEM confirms the successful stepwise surface modification of Fe_3O_4 nanoparticles with functional polymers, enhancing their applicability in biomedical and environmental applications.

Furthermore, the thermo- and pH-responsive behavior of the PIA-b-PNIPAM@Fe_3O_4 composite was investigated using DLS across temperatures (25–45°C) and *pH* values. Given PNIPAM's LCST (~32°C), changes in hydrodynamic diameter were monitored to track the phase transitions of the composite. Figure 4 illustrates how the effective hydrodynamic diameter of the PIA-b-PNIPAM@Fe_3O_4 changes with temperature and pH, offering valuable insights into the dual

 doi:10.20944/preprints202505.1553.v1

environmental responsiveness of the nanocomposite. A substantial 45% reduction in hydrodynamic diameter was observed as temperature increased at neutral *pH* (*pH* 7), a phenomenon attributed to the thermoresponsive collapse of the PNIPAM shell above its LCST. Below 32 °C, PNIPAM adopts a hydrated, extended coil conformation due to strong hydrogen bonding between the polymer chains and surrounding water molecules. However, as the temperature surpasses the LCST, PNIPAM undergoes a coil-to-globule transition, expelling water from the polymer matrix and collapsing into a more compact structure, thereby reducing the overall nanoparticle size.

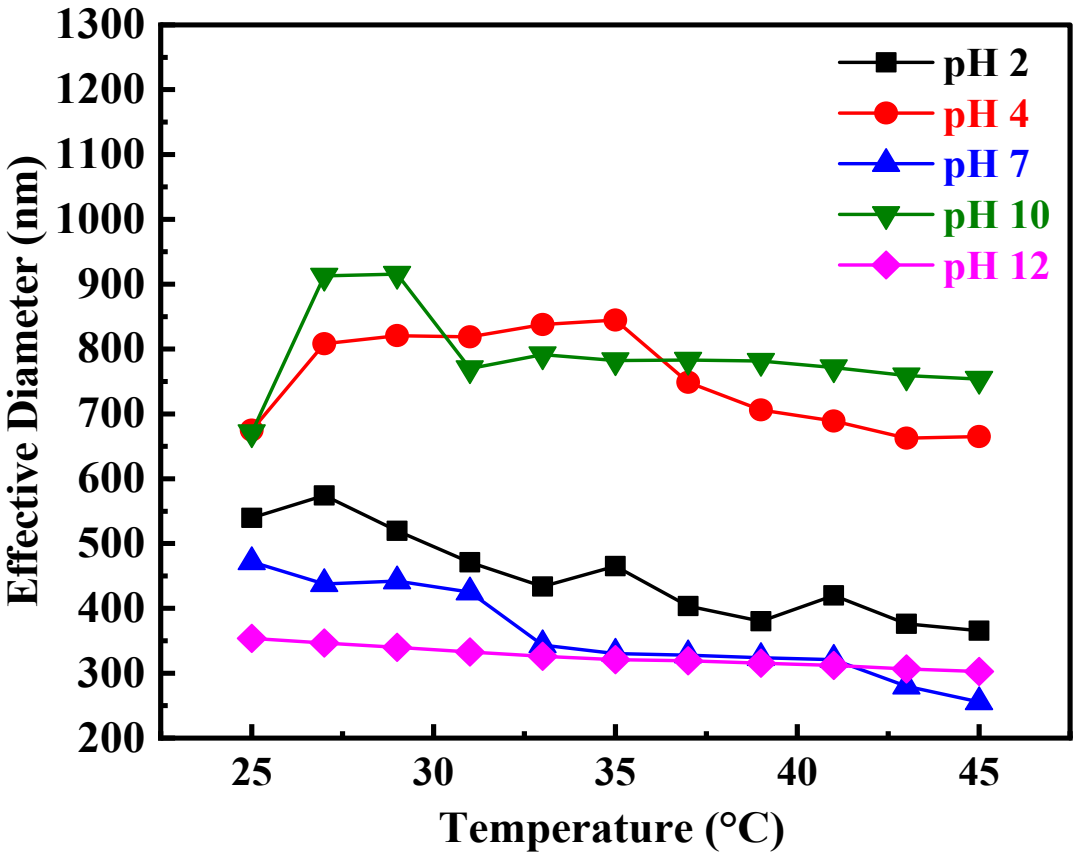

Figure 4. Effect of temperature and *pH* on effective dimeter of PIA-b-PNIPAM @Fe_3O_4 stimuli-responsive polymer composite measured from DLS.

The observed *pH* and temperature-dependent behavior of the nanocomposite is rooted in the interplay between polymer protonation states and the thermoresponsive nature of PNIPAM. At a highly acidic *pH* of 2, the carboxyl groups in PIA become protonated, converting $–COO^-$ groups into –COOH. This protonation reduces the net negative charge along the polymer chains, thereby diminishing electrostatic repulsion between them. Consequently, when the temperature is raised to 45°C, the PNIPAM segments again undergo a coil-to-globule transition, leading to a pronounced contraction of the polymer shell—a 32.32% reduction in hydrodynamic size.

In contrast, at *pH* 12, the carboxyl groups remain deprotonated and exist as $–COO^-$, which imparts a higher negative charge density along the PIA chains. This enhanced charge leads to increased electrostatic repulsion, which tends to keep the polymer chains in a more extended conformation. As a result, when the temperature increases, the typical thermoresponsive collapse of PNIPAM is partially counteracted by these repulsive forces, resulting in a comparatively smaller reduction in particle size—only 14.35%. At *pH* 4, the hydrodynamic diameter remained nearly unchanged, with only a minimal 1.49% reduction, indicating that the polymer network retained its hydration and structural integrity due to partial protonation of PIA, which prevented significant chain contraction. Conversely, at *pH* 10, an unexpected 12.32% increase in nanoparticle size was

 doi:10.20944/preprints202505.1553.v1

observed, suggesting that ionization of functional groups at this *pH* level led to electrostatic repulsion-driven polymer expansion.

Furthermore, temperature-dependent size reduction in hydrodynamic diameter was observed across all *pH* values below 10, confirming the strong influence of PNIPAM's thermoresponsive behavior. However, at *pH* 10, the nanoparticles reached a critical stability point where size remained unaffected by further temperature changes. This behavior likely stems from an equilibrium between electrostatic repulsion and polymer solubility, effectively suppressing the typical LCST-driven collapse of PNIPAM. These findings underscore the dual-responsive nature of PIA-b-PNIPAM@Fe_3O_4 composite, which exhibits tunable swelling and deswelling properties depending on temperature and *pH*. Such adaptability makes them highly promising for applications in controlled drug delivery, stimuli-responsive nanocarriers, and environmental sensing, where precise regulation of nanoparticle size and stability is essential.

Eyiler and Walters synthesized and characterized superparamagnetic Fe_3O_4 nanoparticles functionalized with a dual-responsive block copolymer, PIA-b-PNIPAM, via aqueous SI-ATRP[63]. The resulting Fe_3O_4–PIA-b-PNIPAM nanocomposites demonstrated clear temperature-responsive behavior, with a size reduction of approximately 20 nm between 25 °C and 34 °C, and the phase transition was observed around 32 °C, corresponding to PNIPAM's LCST. In comparison, this present study represents an improvement over the previous work[63], achieving a more pronounced- 45% reduction in hydrodynamic size between 25–45 °C at neutral pH. Additionally, the current system reveals pH-dependent responsiveness, with significant swelling-shrinking behaviors at *pH* 2 and 12 but minimal variation below *pH* 10. This enhanced dual-stimuli responsiveness indicates greater tunability compared to previous reports. While both studies used similar analytical approaches and confirmed PNIPAM's reversible transition from a hydrophilic to a hydrophobic state upon heating, the observed differences are attributed to variations in grafting density, particle size, surface modification of SPIONPs via APTES, and the extent of magnetization reduction due to polymer coatings. Collectively, these findings highlight the promise of PNIPAM-functionalized nanocomposites for dual stimuli-responsive drug delivery and biomedical applications.

4. Conclusions

A dual-responsive block copolymer comprising poly(itaconic acid) (PIA) and poly(N-isopropylacrylamide) (PNIPAM) was successfully grafted onto the surface of the APTES-functionalized Fe_3O_4 nanoparticles with an average diameter of a ~208.54 nm using a hydrothermal method, ensuring uniform size distribution and surface functionalization. The structural and physicochemical properties of the nanoparticles were comprehensively characterized using transmission electron microscopy (TEM), Fourier transform infrared spectroscopy (FTIR), and dynamic light scattering (DLS). FTIR verified successful silanization of the nanoparticle surface by detecting characteristic Si–O–Fe and $–NH_2$ functional groups, indicative of effective APTES (3-aminopropyltriethoxysilane) coating. The polymer grafting was also confirmed through FTIR spectra showing characteristic vibrational peaks of both PIA (carboxylic groups) and PNIPAM (amide and isopropyl groups). The DLS results revealed that the polymer-grafted magnetic nanoparticles exhibited excellent dispersion and stability in aqueous and selected organic solvents, attributed to the hydrophilic nature of the grafted polymer chains and the electrostatic repulsion provided by carboxylic groups. Temperature responsiveness was assessed by monitoring changes in hydrodynamic diameter across varying temperatures at constant pH. A clear thermoresponsive behavior was observed at different pH: increasing temperature led to a reduction in particle size due to the collapse of PNIPAM chains above their lower critical solution temperature (LCST), resulting in a more compact nanocomposite. However, under alkaline conditions (*pH* ≥ 10), the effective diameter remained relatively stable even with temperature elevation, likely due to electrostatic repulsion among deprotonated carboxylate groups in the PIA segments, which counteracted the thermally induced collapse of PNIPAM. These dual-responsive polymers, capable of responding to

 doi:10.20944/preprints202505.1553.v1

changes in both temperature and pH, hold significant promise for applications in smart drug delivery and various biomedical fields.

Data Availability Statement: The data presented in this study are available on request from the corresponding authors.

Acknowledgement: The authors gratefully acknowledge Cayla Cook and Erick Vasquez for their dedicated support and valuable contributions to this research.

Conflicts of Interest: The authors declare no conflicts of interest.

References

1. Lochhead, R. The Use of Polymers in Cosmetic Products. *Cosmet. Sci. Technol. Theor. Princ. Appl.* **2017**, *13*, 171–221.
2. Yusuf, M.; Eskandarinezhad, S. Journal of Composites and Compounds. *J. Compos. Compd.* **2021**, *3*, 275–290.
3. Sharma, S.; Sudhakara, P.; Omran, A. A. B.; Singh, J.; Ilyas, R. Recent Trends and Developments in Conducting Polymer Nanocomposites for Multifunctional Applications. *Polymers* **2021**, *13* (17), 2898.
4. Sadasivuni, K. K.; Hegazy, S. M.; Aly, Aa. A. M. A.; Waseem, S.; Karthik, K. Polymers in Electronics. In *Polymer science and innovative applications*; Elsevier, 2020; pp 365–392.
5. Chen, Y.; Liu, G.; Wang, C.; Zhang, W.; Li, R.-W.; Wang, L. Polymer Memristor for Information Storage and Neuromorphic Applications. *Mater. Horiz.* **2014**, *1* (5), 489–506.
6. Ikada, Y. Surface Modification of Polymers for Medical Applications. *Biomaterials* **1994**, *15* (10), 725–736.
7. Sharma, S.; Sudhakara, P.; Omran, A. A. B.; Singh, J.; Ilyas, R. Recent Trends and Developments in Conducting Polymer Nanocomposites for Multifunctional Applications. *Polymers* **2021**, *13* (17), 2898.
8. Moinudeen, G.; Ahmad, F.; Kumar, D.; Al-Douri, Y.; Ahmad, S. IoT Applications in Future Foreseen Guided by Engineered Nanomaterials and Printed Intelligence Technologies a Technology Review. *Int. J. Internet Things* **2017**, *6* (3), 106–148.
9. Mao Png, Z.; Wang, C.-G.; Chuan Yeo, J. C.; Cheng Lee, J. J.; Erdeanna Surat'man, N.; Lin Tan, Y.; Liu, H.; Wang, P.; Hoon Tan, B.; Wei Xu, J.; Jun Loh, X.; Zhu, Q. Stimuli-Responsive Structure–Property Switchable Polymer Materials. *Mol. Syst. Des. Eng.* **2023**, *8* (9), 1097–1129. https://doi.org/10.1039/D3ME00002H.
10. Hiruta, Y. Poly(N-Isopropylacrylamide)-Based Temperature- and pH-Responsive Polymer Materials for Application in Biomedical Fields. *Polym. J.* **2022**, *54* (12), 1419–1430. https://doi.org/10.1038/s41428-022-00687-z.
11. Elliott, J. E.; Macdonald, M.; Nie, J.; Bowman, C. N. Structure and Swelling of Poly(Acrylic Acid) Hydrogels: Effect of pH, Ionic Strength, and Dilution on the Crosslinked Polymer Structure. *Polymer* **2004**, *45* (5), 1503–1510. https://doi.org/10.1016/j.polymer.2003.12.040.
12. Swift, T.; Swanson, L.; Geoghegan, M.; Rimmer, S. The pH-Responsive Behaviour of Poly(Acrylic Acid) in Aqueous Solution Is Dependent on Molar Mass. *Soft Matter* **2016**, *12* (9), 2542–2549. https://doi.org/10.1039/C5SM02693H.
13. Shu, T.; Hu, L.; Shen, Q.; Jiang, L.; Zhang, Q.; Serpe, M. J. Stimuli-Responsive Polymer-Based Systems for Diagnostic Applications. *J. Mater. Chem. B* **2020**, *8* (32), 7042–7061. https://doi.org/10.1039/D0TB00570C.
14. Trehan, K.; Saini, M.; Thakur, S. Stimuli-Responsive Material in Controlled Release of Drug. In *Engineered Biomaterials: Synthesis and Applications*; Malviya, R., Sundram, S., Eds.; Springer Nature: Singapore, 2023; pp 535–561. https://doi.org/10.1007/978-981-99-6698-1_18.
15. Wagay, Z. A.; Rongpi, S. Stimuli-Responsive In-Situ Gelling Systems: Smart Polymers for Enhanced Drug Delivery.
16. Ahadi, F.; Bahmanpour, A. H.; Mozafari, M. 14 - Stimuli-Responsive Polymers for Biomedical Applications. In *Handbook of Polymers in Medicine*; Mozafari, M., Singh Chauhan, N. P., Eds.; Woodhead Publishing Series in Biomaterials; Woodhead Publishing, 2023; pp 401–423. https://doi.org/10.1016/B978-0-12-823797-7.00014-9.

 doi:10.20944/preprints202505.1553.v1

17. Zhang, A.; Jung, K.; Li, A.; Liu, J.; Boyer, C. Recent Advances in Stimuli-Responsive Polymer Systems for Remotely Controlled Drug Release. *Prog. Polym. Sci.* **2019**, *99*, 101164. https://doi.org/10.1016/j.progpolymsci.2019.101164.
18. Municoy, S.; Álvarez Echazú, M. I.; Antezana, P. E.; Galdopórpora, J. M.; Olivetti, C.; Mebert, A. M.; Foglia, M. L.; Tuttolomondo, M. V.; Alvarez, G. S.; Hardy, J. G.; Desimone, M. F. Stimuli-Responsive Materials for Tissue Engineering and Drug Delivery. *Int. J. Mol. Sci.* **2020**, *21* (13), 4724. https://doi.org/10.3390/ijms21134724.
19. Shi, J.; Yu, L.; Ding, J. PEG-Based Thermosensitive and Biodegradable Hydrogels. *Acta Biomater.* **2021**, *128*, 42–59. https://doi.org/10.1016/j.actbio.2021.04.009.
20. Alexander, A.; Ajazuddin; Khan, J.; Saraf, S.; Saraf, S. Polyethylene Glycol (PEG)–Poly(N-Isopropylacrylamide) (PNIPAAm) Based Thermosensitive Injectable Hydrogels for Biomedical Applications. *Eur. J. Pharm. Biopharm.* **2014**, *88* (3), 575–585. https://doi.org/10.1016/j.ejpb.2014.07.005.
21. Dhawan, S.; Dhawan, K.; Varma, M.; Sinha, V. Applications of Poly (Ethylene Oxide) in Drug Delivery Systems. *Pharm Technol* **2005**, *29*, 82–96.
22. Chiu, H.-C.; Hsiue ,Ging-Ho; Lee ,Yang-Ping; and Huang, L.-W. Synthesis and Characterization of pH-Sensitive Dextran Hydrogels as a Potential Colon-Specific Drug Delivery System. *J. Biomater. Sci. Polym. Ed.* **1999**, *10* (5), 591–608. https://doi.org/10.1163/156856299X00504.
23. Guo, Y.; Sun ,Jihong; Bai ,Shiyang; and Wu, X. pH-Sensitive Performance of Dextran–Poly(Acrylic Acid) Copolymer and Its Application in Controlled in Vitro Release of Ibuprofen. *Int. J. Polym. Mater. Polym. Biomater.* **2017**, *66* (17), 900–906. https://doi.org/10.1080/00914037.2017.1291509.
24. Bardajee, G. R.; Hooshyar, Z.; Rastgo, F. Kappa Carrageenan-g-Poly (Acrylic Acid)/SPION Nanocomposite as a Novel Stimuli-Sensitive Drug Delivery System. *Colloid Polym. Sci.* **2013**, *291* (12), 2791–2803. https://doi.org/10.1007/s00396-013-3018-6.
25. Luo, T.; Lin, S.; Xie, R.; Ju, X.-J.; Liu, Z.; Wang, W.; Mou, C.-L.; Zhao, C.; Chen, Q.; Chu, L.-Y. pH-Responsive Poly(Ether Sulfone) Composite Membranes Blended with Amphiphilic Polystyrene-*Block*-Poly(Acrylic Acid) Copolymers. *J. Membr. Sci.* **2014**, *450*, 162–173. https://doi.org/10.1016/j.memsci.2013.09.002.
26. Vega-Chacón, J.; Arbeláez, M. I. A.; Jorge, J. H.; Marques, R. F. C.; Jafelicci, M. pH-Responsive Poly(Aspartic Acid) Hydrogel-Coated Magnetite Nanoparticles for Biomedical Applications. *Mater. Sci. Eng. C* **2017**, *77*, 366–373. https://doi.org/10.1016/j.msec.2017.03.244.
27. Yang, P.; Li, D.; Jin, S.; Ding, J.; Guo, J.; Shi, W.; Wang, C. Stimuli-Responsive Biodegradable Poly(Methacrylic Acid) Based Nanocapsules for Ultrasound Traced and Triggered Drug Delivery System. *Biomaterials* **2014**, *35* (6), 2079–2088. https://doi.org/10.1016/j.biomaterials.2013.11.057.
28. Ye, M.; Zhang, D.; Han, L.; Tejada, J.; Ortiz, C. Synthesis, Preparation, and Conformation of Stimulus-Responsive End-Grafted Poly(Methacrylic Acid-g-Ethylene Glycol) Layers. *Soft Matter* **2006**, *2* (3), 243–256. https://doi.org/10.1039/B510894B.
29. Hebishima, T.; Yuba, E.; Kono, K.; Takeshima, S.; Ito, Y.; Aida, Y. The pH-Sensitive Fusogenic 3-Methyl-Glutarylated Hyperbranched Poly(Glycidol)-Conjugated Liposome Induces Antigen-Specific Cellular and Humoral Immunity. *Clin. Vaccine Immunol.* **2012**, *19* (9), 1492–1498. https://doi.org/10.1128/CVI.00273-12.
30. Zhang, Y.; Kim, I.; Lu, Y.; Xu, Y.; Yu, D.-G.; Song, W. Intelligent Poly(l-Histidine)-Based Nanovehicles for Controlled Drug Delivery. *J. Controlled Release* **2022**, *349*, 963–982. https://doi.org/10.1016/j.jconrel.2022.08.005.
31. Rey, M.; Fernandez-Rodriguez, M. A.; Karg, M.; Isa, L.; Vogel, N. Poly-N-Isopropylacrylamide Nanogels and Microgels at Fluid Interfaces. *Acc. Chem. Res.* **2020**, *53* (2), 414–424.
32. Najafi, M.; Hebels, E.; Hennink, W. E.; Vermonden, T. Poly (N-isopropylacrylamide): Physicochemical Properties and Biomedical Applications. *Temp. Polym. Chem. Prop. Appl.* **2018**, 1–34.
33. Shaibie, N. A.; Ramli, N. A.; Mohammad Faizal, N. D. F.; Srichana, T.; Mohd Amin, M. C. I. Poly (N-isopropylacrylamide)-Based Polymers: Recent Overview for the Development of Temperature-Responsive Drug Delivery and Biomedical Applications. *Macromol. Chem. Phys.* **2023**, *224* (20), 2300157.
34. *Active Control of SPR by Thermoresponsive Hydrogels for Biosensor Applications | The Journal of Physical Chemistry C*. https://pubs.acs.org/doi/full/10.1021/jp400255u (accessed 2025-05-10).

 doi:10.20944/preprints202505.1553.v1

35. Toma, M.; Jonas, U.; Mateescu, A.; Knoll, W.; Dostalek, J. Active Control of SPR by Thermoresponsive Hydrogels for Biosensor Applications. *J. Phys. Chem. C* **2013**, *117* (22), 11705–11712. https://doi.org/10.1021/jp400255u.
36. Tang, L.; Wang, L.; Yang, X.; Feng, Y.; Li, Y.; Feng, W. Poly(*N*-Isopropylacrylamide)-Based Smart Hydrogels: Design, Properties and Applications. *Prog. Mater. Sci.* **2021**, *115*, 100702. https://doi.org/10.1016/j.pmatsci.2020.100702.
37. Tekin, H.; Sanchez, J. G.; Tsinman, T.; Langer, R.; Khademhosseini, A. Thermoresponsive Platforms for Tissue Engineering and Regenerative Medicine. *AIChE J. Am. Inst. Chem. Eng.* **2011**, *57* (12), 3249–3258. https://doi.org/10.1002/aic.12801.
38. Uthman, H. Advances in Membranes for High Temperature Polymer Electrolyte Membrane Fuel Cells; 2013; pp 1–25.
39. VINCE, M.; AUGUSTYNIAK, A.; Durant, Y.; Shaw, J. Soluble Aqueous Compositions of Selected Polyitaconic Acid Polymers. WO2015100412A1, July 2, 2015. https://patents.google.com/patent/WO2015100412A1/en (accessed 2025-05-10).
40. Lanzalaco, S.; Armelin, E. Poly(N-Isopropylacrylamide) and Copolymers: A Review on Recent Progresses in Biomedical Applications. *Gels* **2017**, *3* (4), 36. https://doi.org/10.3390/gels3040036.
41. Gao, Z.; Tao, X.; Cui, Y.; Satoh, T.; Kakuchi, T.; Duan, Q. Synthesis of End-Functionalized Poly(N -Isopropylacrylamide) with Group of Asymmetrical Phthalocyanine via Atom Transfer Radical Polymerization and Its Photocatalytic Oxidation of Rhodamine B. *Polym. Chem.* **2011**, *2* (11), 2590–2596. https://doi.org/10.1039/C1PY00308A.
42. Qiu, J.; Charleux, B.; Matyjaszewski, K. Controlled/Living Radical Polymerization in Aqueous Media: Homogeneous and Heterogeneous Systems. *Prog. Polym. Sci.* **2001**, *26* (10), 2083–2134. https://doi.org/10.1016/S0079-6700(01)00033-8.
43. Khabibullin, A.; Mastan, E.; Matyjaszewski, K.; Zhu, S. Surface-Initiated Atom Transfer Radical Polymerization. In *Controlled Radical Polymerization at and from Solid Surfaces*; Vana, P., Ed.; Springer International Publishing: Cham, 2016; pp 29–76. https://doi.org/10.1007/12_2015_311.
44. Yar, Y.; Khodadust, R.; Akkoc, Y.; Utkur, M.; Saritas, E. U.; Gozuacik, D.; Acar, H. Y. Development of Tailored SPION-PNIPAM Nanoparticles by ATRP for Dually Responsive Doxorubicin Delivery and MR Imaging. *J. Mater. Chem. B* **2018**, *6* (2), 289–300. https://doi.org/10.1039/C7TB00646B.
45. Shi, Y.; Chen, Z. Function-Driven Design of Stimuli-Responsive Polymer Composites: Recent Progress and Challenges. *J. Mater. Chem. C* **2018**, *6* (44), 11817–11834. https://doi.org/10.1039/C8TC02980F.
46. You, Y.-Z.; Hong, C.-Y.; Pan, C.-Y. Preparation of Smart Polymer/Carbon Nanotube Conjugates via Stimuli-Responsive Linkages. *Adv. Funct. Mater.* **2007**, *17* (14), 2470–2477. https://doi.org/10.1002/adfm.200600742.
47. Majumder, J.; Minko, T. Multifunctional and Stimuli-Responsive Nanocarriers for Targeted Therapeutic Delivery. *Expert Opin. Drug Deliv.* **2021**, *18* (2), 205–227. https://doi.org/10.1080/17425247.2021.1828339.
48. Khakpour, E.; Salehi, S.; Naghib, S. M.; Ghorbanzadeh, S.; Zhang, W. Graphene-Based Nanomaterials for Stimuli-Sensitive Controlled Delivery of Therapeutic Molecules. *Front. Bioeng. Biotechnol.* **2023**, *11*, 1129768. https://doi.org/10.3389/fbioe.2023.1129768.
49. Zhi, D.; Yang, T.; Yang, J.; Fu, S.; Zhang, S. Targeting Strategies for Superparamagnetic Iron Oxide Nanoparticles in Cancer Therapy. *Acta Biomater.* **2020**, *102*, 13–34. https://doi.org/10.1016/j.actbio.2019.11.027.
50. Talelli, M.; Rijcken, C. J. F.; Lammers, T.; Seevinck, P. R.; Storm, G.; van Nostrum, C. F.; Hennink, W. E. Superparamagnetic Iron Oxide Nanoparticles Encapsulated in Biodegradable Thermosensitive Polymeric Micelles: Toward a Targeted Nanomedicine Suitable for Image-Guided Drug Delivery. *Langmuir* **2009**, *25* (4), 2060–2067. https://doi.org/10.1021/la8036499.
51. *Near-infrared light remote-controlled intracellular anti-cancer drug delivery using thermo/pH sensitive nanovehicle - ScienceDirect*. https://www.sciencedirect.com/science/article/pii/S1742706115000367?ref=pdf_download&fr=RR-2&rr=93c9b2507c666162 (accessed 2025-05-10).

 doi:10.20944/preprints202505.1553.v1

52. L. Moore, T.; Rodriguez-Lorenzo, L.; Hirsch, V.; Balog, S.; Urban, D.; Jud, C.; Rothen-Rutishauser, B.; Lattuada, M.; Petri-Fink, A. Nanoparticle Colloidal Stability in Cell Culture Media and Impact on Cellular Interactions. *Chem. Soc. Rev.* **2015**, *44* (17), 6287–6305. https://doi.org/10.1039/C4CS00487F.
53. Liu, Y.; Li, Y.; Li, X.-M.; He, T. Kinetics of (3-Aminopropyl)Triethoxylsilane (APTES) Silanization of Superparamagnetic Iron Oxide Nanoparticles. *Langmuir* **2013**, *29* (49), 15275–15282. https://doi.org/10.1021/la403269u.
54. Fu, R.; Yan, Y.; Roberts, C.; Liu, Z.; Chen, Y. The Role of Dipole Interactions in Hyperthermia Heating Colloidal Clusters of Densely-Packed Superparamagnetic Nanoparticles. *Sci. Rep.* **2018**, *8* (1), 4704. https://doi.org/10.1038/s41598-018-23225-5.
55. Laurent, S.; Mahmoudi, M. Superparamagnetic Iron Oxide Nanoparticles: Promises for Diagnosis and Treatment of Cancer. *Int. J. Mol. Epidemiol. Genet.* **2011**, *2* (4), 367–390.
56. Wahajuddin; and Arora, S. Superparamagnetic Iron Oxide Nanoparticles: Magnetic Nanoplatforms as Drug Carriers. *Int. J. Nanomedicine* **2012**, *7*, 3445–3471. https://doi.org/10.2147/IJN.S30320.
57. Pucci, C.; Degl'Innocenti, A.; Gümüş, M. B.; Ciofani, G. Superparamagnetic Iron Oxide Nanoparticles for Magnetic Hyperthermia: Recent Advancements, Molecular Effects, and Future Directions in the Omics Era. *Biomater. Sci.* **2022**, *10* (9), 2103–2121. https://doi.org/10.1039/D1BM01963E.
58. Rahman, M. Magnetic Resonance Imaging and Iron-Oxide Nanoparticles in the Era of Personalized Medicine. *Nanotheranostics* **2023**, *7* (4), 424–449. https://doi.org/10.7150/ntno.86467.
59. Gonçalves, A. I.; Miranda, M. S.; Rodrigues, M. T.; Reis, R. L.; Gomes, M. E. Magnetic Responsive Cell-Based Strategies for Diagnostics and Therapeutics. *Biomed. Mater.* **2018**, *13* (5), 054001. https://doi.org/10.1088/1748-605X/aac78b.
60. *Full article: Superparamagnetic iron oxide nanoparticles: magnetic nanoplatforms as drug carriers*. https://www.tandfonline.com/doi/full/10.2147/IJN.S30320 (accessed 2025-05-10).
61. Ramanujan, R. V.; Ang, K. L.; Venkatraman, S. Magnet–PNIPA Hydrogels for Bioengineering Applications. *J. Mater. Sci.* **2009**, *44* (5), 1381–1387. https://doi.org/10.1007/s10853-006-1064-x.
62. Karthika, V.; AlSalhi, M. S.; Devanesan, S.; Gopinath, K.; Arumugam, A.; Govindarajan, M. Chitosan Overlaid Fe3O4/rGO Nanocomposite for Targeted Drug Delivery, Imaging, and Biomedical Applications. *Sci. Rep.* **2020**, *10* (1), 18912. https://doi.org/10.1038/s41598-020-76015-3.
63. Eyiler, E.; Walters, K. B. Magnetic Iron Oxide Nanoparticles Grafted with Poly (Itaconic Acid)-Block-Poly (N-Isopropylacrylamide). *Colloids Surf. Physicochem. Eng. Asp.* **2014**, *444*, 321–325.
64. Conzatti, G.; Chamary, S.; De Geyter, N.; Cavalie, S.; Morent, R.; Tourrette, A. Surface Functionalization of Plasticized Chitosan Films through PNIPAM Grafting via UV and Plasma Graft Polymerization. *Eur. Polym. J.* **2018**, *105*, 434–441.
65. Kakar, M. U.; Khan, K.; Akram, M.; Sami, R.; Khojah, E.; Iqbal, I.; Helal, M.; Hakeem, A.; Deng, Y.; Dai, R. Synthesis of Bimetallic Nanoparticles Loaded on to PNIPAM Hybrid Microgel and Their Catalytic Activity. *Sci. Rep.* **2021**, *11* (1), 14759.
66. Huerta-Ángeles, G.; Kanizsová, L.; Mielczarek, K.; Konefał, M.; Konefał, R.; Hodan, J.; Kočková, O.; Bednarz, S.; Beneš, H. Sustainable Aerogels Based on Biobased Poly (Itaconic Acid) for Adsorption of Cationic Dyes. *Int. J. Biol. Macromol.* **2024**, *259*, 129727.
67. Ghorbani, M.; Hamishehkar, H.; Arsalani, N.; Entezami, A. A. Surface Decoration of Magnetic Nanoparticles with Folate-Conjugated Poly (N-Isopropylacrylamide-Co-Itaconic Acid): A Facial Synthesis of Dual-Responsive Nanocarrier for Targeted Delivery of Doxorubicin. *Int. J. Polym. Mater. Polym. Biomater.* **2016**, *65* (13), 683–694.
68. Anushree, C.; Krishna, D. N. G.; Philip, J. Synthesis of Ni Doped Iron Oxide Colloidal Nanocrystal Clusters Using Poly (N-Isopropylacrylamide) Templates for Efficient Recovery of Cefixime and Methylene Blue. *Colloids Surf. Physicochem. Eng. Asp.* **2022**, *650*, 129616.
69. Sakai, R.; Matsuyama, T.; Ida, J. Effect of Immobilization Method and Particle Size on Heavy Metal Ion Recovery of Thermoresponsive Polymer/Magnetic Particle Composites. *Colloids Surf. Physicochem. Eng. Asp.* **2020**, *590*, 124499.

 doi:10.20944/preprints202505.1553.v1

70. Mohamed, A. L.; Hassabo, A. G. Core–Shell Titanium@ Silica Nanoparticles Impregnating in Poly (Itaconic Acid)/Poly (N-Isopropylacrylamide) Microgel for Multifunctional Cellulosic Fabrics. *J. Polym. Res.* **2022**, *29* (2), 68.
71. *11.5: Infrared Spectra of Some Common Functional Groups*. Chemistry LibreTexts. https://chem.libretexts.org/Bookshelves/Organic_Chemistry/Map%3A_Organic_Chemistry_(Wade)_Complete_and_Semesters_I_and_II/Map%3A_Organic_Chemistry_(Wade)/11%3A_Infrared_Spectroscopy_and_Mass_Spectrometry/11.05%3A_Infrared_Spectra_of_Some_Common_Functional_Groups (accessed 2025-05-11).